Search for η and η^{′} invisible decays in J/ψ→φη and φη^{′}

M. Ablikim *et al.* (BESIII Collaboration)

Search for η and η' Invisible Decays in $J/\psi \to \phi\eta$ and $\phi\eta'$

M. Ablikim[1], M. N. Achasov[6], O. Albayrak[3], D. J. Ambrose[39], F. F. An[1], Q. An[40], J. Z. Bai[1], Y. Ban[26], J. Becker[2], J. V. Bennett[16], M. Bertani[17A], J. M. Bian[38], E. Boger[19,a], O. Bondarenko[20], I. Boyko[19], R. A. Briere[3], V. Bytev[19], X. Cai[1], O. Cakir[34A], A. Calcaterra[17A], G. F. Cao[1], S. A. Cetin[34B], J. F. Chang[1], G. Chelkov[19,a], G. Chen[1], H. S. Chen[1], J. C. Chen[1], M. L. Chen[1], S. J. Chen[24], X. Chen[26], Y. B. Chen[1], H. P. Cheng[14], Y. P. Chu[1], D. Cronin-Hennessy[38], H. L. Dai[1], J. P. Dai[1], D. Dedovich[19], Z. Y. Deng[1], A. Denig[18], I. Denysenko[19,b], M. Destefanis[43A,43C], W. M. Ding[28], Y. Ding[22], L. Y. Dong[1], M. Y. Dong[1], S. X. Du[46], J. Fang[1], S. S. Fang[1], L. Fava[43B,43C], C. Q. Feng[40], R. B. Ferroli[17A], P. Friedel[2], C. D. Fu[1], J. L. Fu[24], Y. Gao[33], C. Geng[40], K. Goetzen[7], W. X. Gong[1], W. Gradl[18], M. Greco[43A,43C], M. H. Gu[1], Y. T. Gu[9], Y. H. Guan[36], A. Q. Guo[25], L. B. Guo[23], T. Guo[23], Y. P. Guo[25], Y. L. Han[1], F. A. Harris[37], K. L. He[1], M. He[1], Z. Y. He[25], T. Held[2], Y. K. Heng[1], Z. L. Hou[1], C. Hu[23], H. M. Hu[1], J. F. Hu[35], T. Hu[1], G. M. Huang[4], G. S. Huang[40], J. S. Huang[12], L. Huang[1], X. T. Huang[28], Y. Huang[24], Y. P. Huang[1], T. Hussain[42], C. S. Ji[40], Q. Ji[1], Q. P. Ji[25], X. B. Ji[1], X. L. Ji[1], L. L. Jiang[1], X. S. Jiang[1], J. B. Jiao[28], Z. Jiao[14], D. P. Jin[1], S. Jin[1], F. F. Jing[33], N. Kalantar-Nayestanaki[20], M. Kavatsyuk[20], B. Kopf[2], M. Kornicer[37], W. Kuehn[35], W. Lai[1], J. S. Lange[35], M. Leyhe[2], C. H. Li[1], Cheng Li[40], Cui Li[40], D. M. Li[46], F. Li[1], G. Li[1], H. B. Li[1], J. C. Li[1], K. Li[10], Lei Li[1], Q. J. Li[1], S. L. Li[1], W. D. Li[1], W. G. Li[1], X. L. Li[28], X. N. Li[1], X. Q. Li[25], X. R. Li[27], Z. B. Li[32], H. Liang[40], Y. F. Liang[30], Y. T. Liang[35], G. R. Liao[33], X. T. Liao[1], D. Lin[11], B. J. Liu[1], C. L. Liu[3], C. X. Liu[1], F. H. Liu[29], Fang Liu[1], Feng Liu[4], H. Liu[1], H. B. Liu[9], H. H. Liu[13], H. M. Liu[1], H. W. Liu[1], J. P. Liu[44], K. Liu[33], K. Y. Liu[22], Kai Liu[36], P. L. Liu[28], Q. Liu[36], S. B. Liu[40], X. Liu[21], Y. B. Liu[25], Z. A. Liu[1], Zhiqiang Liu[1], Zhiqing Liu[1], H. Loehner[20], G. R. Lu[12], H. J. Lu[14], J. G. Lu[1], Q. W. Lu[29], X. R. Lu[36], Y. P. Lu[1], C. L. Luo[23], M. X. Luo[45], T. Luo[37], X. L. Luo[1], M. Lv[1], C. L. Ma[36], F. C. Ma[22], H. L. Ma[1], Q. M. Ma[1], S. Ma[1], T. Ma[1], X. Y. Ma[1], F. E. Maas[11], M. Maggiora[43A,43C], Q. A. Malik[42], Y. J. Mao[26], Z. P. Mao[1], J. G. Messchendorp[20], J. Min[1], T. J. Min[1], R. E. Mitchell[16], X. H. Mo[1], C. Morales Morales[11], N. Yu. Muchnoi[6], H. Muramatsu[39], Y. Nefedov[19], C. Nicholson[36], I. B. Nikolaev[6], Z. Ning[1], S. L. Olsen[27], Q. Ouyang[1], S. Pacetti[17B], J. W. Park[27], M. Pelizaeus[2], H. P. Peng[40], K. Peters[7], J. L. Ping[23], R. G. Ping[1], R. Poling[38], E. Prencipe[18], M. Qi[24], S. Qian[1], C. F. Qiao[36], L. Q. Qin[28], X. S. Qin[1], Y. Qin[26], Z. H. Qin[1], J. F. Qiu[1], K. H. Rashid[42], G. Rong[1], X. D. Ruan[9], A. Sarantsev[19,c], B. D. Schaefer[16], M. Shao[40], C. P. Shen[37,d], X. Y. Shen[1], H. Y. Sheng[1], M. R. Shepherd[16], X. Y. Song[1], S. Spataro[43A,43C], B. Spruck[35], D. H. Sun[1], G. X. Sun[1], J. F. Sun[12], S. S. Sun[1], Y. J. Sun[40], Y. Z. Sun[1], Z. J. Sun[1], Z. T. Sun[40], C. J. Tang[30], X. Tang[1], I. Tapan[34C], E. H. Thorndike[39], D. Toth[38], M. Ullrich[35], G. S. Varner[37], B. Q. Wang[26], D. Wang[26], D. Y. Wang[26], K. Wang[1], L. L. Wang[1], L. S. Wang[1], M. Wang[28], P. Wang[1], P. L. Wang[1], Q. J. Wang[1], S. G. Wang[26], X. F. Wang[33], X. L. Wang[40], Y. D. Wang[17A], Y. F. Wang[1], Y. Q. Wang[18], Z. Wang[1], Z. G. Wang[1], Z. Y. Wang[1], D. H. Wei[8], J. B. Wei[26], P. Weidenkaff[18], Q. G. Wen[40], S. P. Wen[1], M. Werner[35], U. Wiedner[2], L. H. Wu[1], N. Wu[1], S. X. Wu[40], W. Wu[25], Z. Wu[1], L. G. Xia[33], Y. X Xia[15], Z. J. Xiao[23], Y. G. Xie[1], Q. L. Xiu[1], G. F. Xu[1], G. M. Xu[26], Q. J. Xu[10], Q. N. Xu[36], X. P. Xu[31], Z. R. Xu[40], F. Xue[4], Z. Xue[1], L. Yan[40], W. B. Yan[40], Y. H. Yan[15], H. X. Yang[1], Y. Yang[4], Y. X. Yang[8], H. Ye[1], M. Ye[1], M. H. Ye[5], B. X. Yu[1], C. X. Yu[25], H. W. Yu[26], J. S. Yu[21], S. P. Yu[28], C. Z. Yuan[1], Y. Yuan[1], A. A. Zafar[42], A. Zallo[17A], Y. Zeng[15], B. X. Zhang[1], B. Y. Zhang[1], C. Zhang[24], C. C. Zhang[1], D. H. Zhang[1], H. H. Zhang[32], H. Y. Zhang[1], J. Q. Zhang[1], J. W. Zhang[1], J. Y. Zhang[1], J. Z. Zhang[1], LiLi Zhang[15], R. Zhang[36], S. H. Zhang[1], X. J. Zhang[1], X. Y. Zhang[28], Y. Zhang[1], Y. H. Zhang[1], Z. P. Zhang[40], Z. Y. Zhang[44], Zhenghao Zhang[4], G. Zhao[1], H. S. Zhao[1], J. W. Zhao[1], K. X. Zhao[23], Lei Zhao[40], Ling Zhao[1], M. G. Zhao[25], Q. Zhao[1], Q. Z. Zhao[9], S. J. Zhao[46], T. C. Zhao[1], X. H. Zhao[24], Y. B. Zhao[1], Z. G. Zhao[40], A. Zhemchugov[19,a], B. Zheng[41], J. P. Zheng[1], Y. H. Zheng[36], B. Zhong[23], Z. Zhong[9], L. Zhou[1], X. K. Zhou[36], X. R. Zhou[40], C. Zhu[1], K. Zhu[1], K. J. Zhu[1], S. H. Zhu[1], X. L. Zhu[33], Y. C. Zhu[40], Y. M. Zhu[25], Y. S. Zhu[1], Z. A. Zhu[1], J. Zhuang[1], B. S. Zou[1], J. H. Zou[1]

(BESIII Collaboration)

[1] *Institute of High Energy Physics, Beijing 100049, People's Republic of China*
[2] *Bochum Ruhr-University, D-44780 Bochum, Germany*
[3] *Carnegie Mellon University, Pittsburgh, Pennsylvania 15213, USA*
[4] *Central China Normal University, Wuhan 430079, People's Republic of China*
[5] *China Center of Advanced Science and Technology, Beijing 100190, People's Republic of China*
[6] *G.I. Budker Institute of Nuclear Physics SB RAS (BINP), Novosibirsk 630090, Russia*
[7] *GSI Helmholtzcentre for Heavy Ion Research GmbH, D-64291 Darmstadt, Germany*
[8] *Guangxi Normal University, Guilin 541004, People's Republic of China*
[9] *GuangXi University, Nanning 530004, People's Republic of China*
[10] *Hangzhou Normal University, Hangzhou 310036, People's Republic of China*
[11] *Helmholtz Institute Mainz, Johann-Joachim-Becher-Weg 45, D-55099 Mainz, Germany*
[12] *Henan Normal University, Xinxiang 453007, People's Republic of China*
[13] *Henan University of Science and Technology, Luoyang 471003, People's Republic of China*
[14] *Huangshan College, Huangshan 245000, People's Republic of China*
[15] *Hunan University, Changsha 410082, People's Republic of China*
[16] *Indiana University, Bloomington, Indiana 47405, USA*
[17] *(A)INFN Laboratori Nazionali di Frascati, I-00044, Frascati, Italy; (B)INFN and University of Perugia, I-06100, Perugia, Italy*
[18] *Johannes Gutenberg University of Mainz, Johann-Joachim-Becher-Weg 45, D-55099 Mainz, Germany*
[19] *Joint Institute for Nuclear Research, 141980 Dubna, Moscow region, Russia*

[20] *KVI, University of Groningen, NL-9747 AA Groningen, The Netherlands*
[21] *Lanzhou University, Lanzhou 730000, People's Republic of China*
[22] *Liaoning University, Shenyang 110036, People's Republic of China*
[23] *Nanjing Normal University, Nanjing 210023, People's Republic of China*
[24] *Nanjing University, Nanjing 210093, People's Republic of China*
[25] *Nankai University, Tianjin 300071, People's Republic of China*
[26] *Peking University, Beijing 100871, People's Republic of China*
[27] *Seoul National University, Seoul, 151-747 Korea*
[28] *Shandong University, Jinan 250100, People's Republic of China*
[29] *Shanxi University, Taiyuan 030006, People's Republic of China*
[30] *Sichuan University, Chengdu 610064, People's Republic of China*
[31] *Soochow University, Suzhou 215006, People's Republic of China*
[32] *Sun Yat-Sen University, Guangzhou 510275, People's Republic of China*
[33] *Tsinghua University, Beijing 100084, People's Republic of China*
[34] *(A)Ankara University, Dogol Caddesi, 06100 Tandogan, Ankara, Turkey; (B)Dogus University, 34722 Istanbul, Turkey; (C)Uludag University, 16059 Bursa, Turkey*
[35] *Universitaet Giessen, D-35392 Giessen, Germany*
[36] *University of Chinese Academy of Sciences, Beijing 100049, People's Republic of China*
[37] *University of Hawaii, Honolulu, Hawaii 96822, USA*
[38] *University of Minnesota, Minneapolis, Minnesota 55455, USA*
[39] *University of Rochester, Rochester, New York 14627, USA*
[40] *University of Science and Technology of China, Hefei 230026, People's Republic of China*
[41] *University of South China, Hengyang 421001, People's Republic of China*
[42] *University of the Punjab, Lahore-54590, Pakistan*
[43] *(A)University of Turin, I-10125, Turin, Italy; (B)University of Eastern Piedmont, I-15121, Alessandria, Italy; (C)INFN, I-10125, Turin, Italy*
[44] *Wuhan University, Wuhan 430072, People's Republic of China*
[45] *Zhejiang University, Hangzhou 310027, People's Republic of China*
[46] *Zhengzhou University, Zhengzhou 450001, People's Republic of China*

[a] *Also at the Moscow Institute of Physics and Technology, Moscow 141700, Russia*
[b] *On leave from the Bogolyubov Institute for Theoretical Physics, Kiev 03680, Ukraine*
[c] *Also at the PNPI, Gatchina 188300, Russia*
[d] *Present address: Nagoya University, Nagoya 464-8601, Japan*

Using a sample of $(225.3 \pm 2.8) \times 10^6$ J/ψ decays collected with the BESIII detector at BEPCII, searches for invisible decays of η and η' in $J/\psi \to \phi\eta$ and $\phi\eta'$ are performed. Decays of $\phi \to K^+K^-$ are used to tag the η and η' decays. No signals above background are found for the invisible decays, and upper limits at the 90% confidence level are determined to be 2.6×10^{-4} for the ratio $\frac{\mathcal{B}(\eta \to \text{invisible})}{\mathcal{B}(\eta \to \gamma\gamma)}$ and 2.4×10^{-2} for $\frac{\mathcal{B}(\eta' \to \text{invisible})}{\mathcal{B}(\eta' \to \gamma\gamma)}$. These limits may be used to constrain light dark matter particles or spin-1 U bosons.

PACS numbers: 13.25.Gv, 13.20.Jf, 14.40.Be

I. INTRODUCTION

Invisible or radiative decays of the J/ψ, Υ and other mesons may be used to search for new physics beyond the Standard Model (SM), in particular for neutral states χ, that could be light dark matter constituents, according to $q\bar{q} \to (\gamma)\chi\chi$ [1–3]. Independently of dark matter, radiative meson decays into γ + invisible allow to look, as for spin-0 axions [4], for light spin-1 particles called U bosons, according to $q\bar{q} \to \gamma + U$, where the U can stay invisible when decaying into $\nu\bar{\nu}$ or other neutral particles [5, 6]. Such J/ψ or $\Upsilon \to \gamma + U$ decays were already searched for long ago [7–9].

Processes involving U bosons and dark matter particles χ may be intimately related, with the U's mediating a new interaction between ordinary (SM) and dark matter particles χ. This may indeed be necessary to ensure for sufficient annihilations of *light* dark matter (LDM) particles [10], proposed as an interpretation for the origin of the 511 keV line from the galactic bulge observed by the INTEGRAL satellite [11, 12].

Conversely, this interaction mediated by U bosons may be responsible for the pair-production of LDM particles through $q\bar{q}$ (or e^+e^-) $\to (\gamma)\chi\chi$. In spite of tentative estimates like $\mathcal{B}(\eta(\eta') \to \chi\chi) \approx 1.4 \times 10^{-4}$ (1.5×10^{-6}) [13], one cannot reliably predict such invisible decay rates of mesons just from the dark matter relic density and annihilation cross-section [3]. In particular a U vectorially coupled to quarks and leptons could be responsible for LDM annihilations, without contributing to invisible decays $\eta(\eta') \to \chi\chi$ [2]; this includes the more specific case of a U boson coupled to SM particles through the electromagnetic current [14], also known as a "dark photon". Annihilations $q\bar{q} \to UU$ may also be a source of invisi-

ble meson decays, especially as the invisible decay mode $U \to \chi\chi$ may be dominant [2]. U exchanges could be responsible for a possible discrepancy between the measured and expected values of $g_\mu - 2$ [6].

It is in any case very interesting to search for such light invisible particles in collider experiments [15]. Many searches for the invisible decays of π^0, η, η', J/ψ and $\Upsilon(1S)$ have been performed [16–20]. Invisible decays of η and η' may originate from $\eta(\eta') \to \chi\chi$ or $U_{\rm inv}U_{\rm inv}$. The resulting informations complement those from J/ψ and Υ decays (constraining different matrix elements, for the b and c quarks), and from π^0 decays (giving access to a smaller phase space and, again, for different matrix elements).

Using 58×10^6 J/ψ events, the BESII experiment obtained a first upper limit $\mathcal{B}(\eta(\eta') \to {\rm invisible})/\mathcal{B}(\eta(\eta') \to \gamma\gamma) < 1.65 \times 10^{-3}$ (6.69×10^{-2}), corresponding to $\mathcal{B}(\eta(\eta') \to {\rm invisible}) < 6.5 \times 10^{-4}$ (1.5×10^{-3}) [17]. Complementary to the BESII results, IceCube set $\mathcal{B}(\eta \to \nu_{e,\tau}\bar{\nu}_{e,\tau}) < 6.1 \times 10^{-4}$ [21] for η decays into SM neutrinos. We present here updated results of searches for the invisible decays of η and η'. The data sample used consists of $(225.3 \pm 2.8) \times 10^6$ J/ψ events [22] collected with the BESIII detector [23] at the BEPCII collider [24].

II. THE BESIII EXPERIMENT AND MONTE CARLO SIMULATION

BEPCII/BESIII [23] is a major upgrade of the BESII experiment at the BEPC accelerator. The design peak luminosity of the double-ring e^+e^- collider, BEPCII, is 10^{33} cm^{-2} s^{-1} at a beam current of 0.93 A. The BESIII detector has a geometrical acceptance of 93% of 4π and consists of four main components: (1) a small-celled, helium-based main draft chamber (MDC) with 43 layers, which provides measurements of ionization energy loss (dE/dx). The average single wire resolution is 135 μm, and the momentum resolution for charged particles with momenta of 1 GeV/c in a 1 T magnetic field is 0.5%; (2) an electromagnetic calorimeter (EMC) made of 6240 CsI (Tl) crystals arranged in a cylindrical shape (barrel) plus two end-caps. For 1.0 GeV photons, the energy resolution is 2.5% in the barrel and 5% in the end-caps, and the position resolution is 6 mm in the barrel and 9 mm in the end-caps; (3) a time-of-flight system (TOF) for particle identification (PID) composed of a barrel part made of two layers with 88 pieces of 5 cm thick, 2.4 m long plastic scintillators in each layer, and two end-caps with 96 fan-shaped, 5 cm thick, plastic scintillators in each end-cap. The time resolution is 80 ps in the barrel, and 110 ps in the end-caps, corresponding to a 2σ K/π separation for momenta up to about 1.0 GeV/c; (4) a muon chamber system made of 1000 m^2 of resistive-plate-chambers arranged in 9 layers in the barrel and 8 layers in the end-caps and incorporated in the return iron of the super-conducting magnet. The position resolution is about 2 cm.

The optimization of the event selection and the estimation of physics backgrounds are performed using Monte Carlo (MC) simulated data samples. The GEANT4-based simulation software BOOST [25] includes the geometric and material description of the BESIII detectors, the detector response and digitization models, as well as the tracking of the detector running conditions and performance. The production of the J/ψ resonance is simulated by the MC event generator KKMC [26]; the known decay modes are generated by EVTGEN [27] with branching ratios set at PDG values [28], while the remaining unknown decay modes are modeled by LUNDCHARM [29].

III. DATA ANALYSIS

A. Analyses for η and $\eta' \to$ invisible

In order to detect invisible η and η' decays, we use $J/\psi \to \phi\eta$ and $\phi\eta'$. These two-body decays provide a very simple event topology, in which the ϕ candidates can be reconstructed easily and cleanly decaying into K^+K^-. The reconstructed ϕ particles can be used to tag η and η' in order to allow a search for their invisible decays. In addition, both the ϕ and $\eta(\eta')$ are given strong boosts in the J/ψ decay, so the directions of the η and η' decays are well defined in the lab system and any decay products can be efficiently detected by the BESIII detector. The missing η and η' can be searched for in the distribution of mass recoiling against the ϕ candidate.

Charged tracks in the BESIII detector are reconstructed using track-induced signals in the MDC. We select tracks that originate within ± 10 cm of the interaction point (IP) in the beam direction and within 1 cm in the plane perpendicular to the beam. The tracks must be within the MDC fiducial volume, $|\cos\theta| < 0.93$ (θ is the polar angle with respect to the e^+ beam direction). Candidate events are required to have only two charged tracks reconstructed with a net charge of zero. For each charged track, information from TOF and dE/dx are combined to calculate $\chi^2_{\rm PID}(i)$ values. With the corresponding number of degree of freedom, we obtain probabilities, Prob$_{\rm PID}(i)$, for the hypotheses that a track is a pion, kaon, or proton, where i ($i = \pi/K/p$) is the particle type. For both kaon candidates, we require Prob$_{\rm PID}(K) >$ Prob$_{\rm PID}(\pi)$. The mass recoiling against the ϕ candidate, $M_\phi^{\rm recoil}$, is calculated using the four-momentum of the incident beams in the lab frame ($p_{\rm lab}^\mu = p_{e^-}^\mu + p_{e^+}^\mu$), and constructing the 4-product $(M_\phi^{\rm recoil})^2 = (p_{\rm lab} - p_{KK})^\mu (p_{\rm lab} - p_{KK})_\mu$, where $p_{KK}^\mu = p_\phi^\mu$ is the sum of the four-momentum of the two charged kaons. The η and η' signal regions in the $M_\phi^{\rm recoil}$ distribution are defined to be within 3σ of the known masses of η and η' [28]. Here, σ is the detector resolution and is 17.8 (9.3) MeV/c^2, which is determined from MC simulation, for $J/\psi \to \phi\eta(\eta')$.

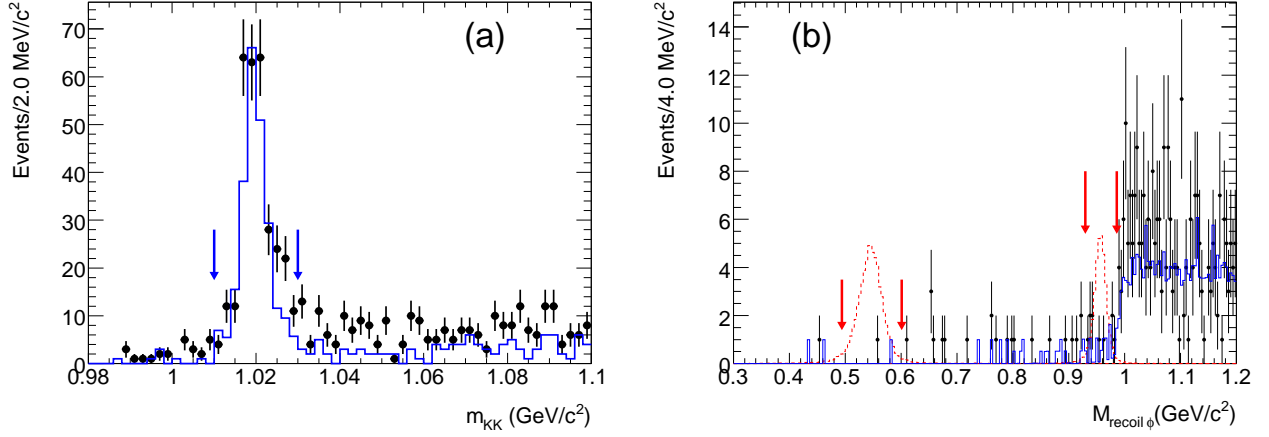Electromagnetic showers are reconstructed from clus-

FIG. 1: (a) The m_{KK} distribution for candidate events in data. The arrows on the plot indicate the signal region of ϕ candidates. Points with error bars are data; the (blue) histogram is expected background. (b) Recoil mass distribution against ϕ candidates, $M_\phi^{\rm recoil}$, for events with 1.01 GeV/$c^2 < m_{KK} < 1.03$ GeV/c^2 in (a). Points with error bars are data; the (blue) solid histogram is the sum of the expected backgrounds; the dashed histograms (with arbitrary scale) are signals of η and η' invisible decays from MC simulations; the arrows on the plot indicate the signal regions of the η and $\eta' \to$ invisible.
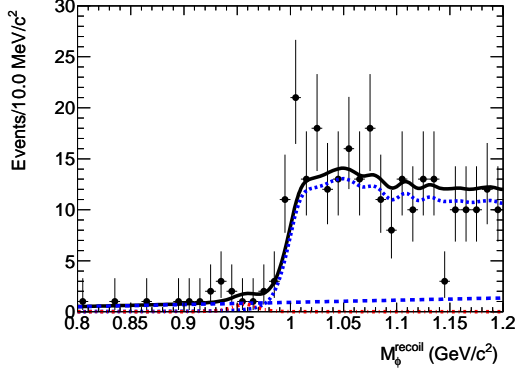

FIG. 2: The $M_\phi^{\rm recoil}$ distribution with events around the η' mass region. Points with error bars are data. The (black) solid curve shows the result of the fit to signal plus background distributions, the (blue) dotted curve shows the background shape from $J/\psi \to \phi f_0(980)(f_0(980) \to K_L K_L)$, the (blue) dashed curve shows the polynomial function for $J/\psi \to \phi K_L K_L$ background, and the (red) dotted-dash curve shows the signal yield.

FIG. 3: The $M_\phi^{\rm recoil}$ distribution for the control sample $J/\psi \to \phi\eta'$, $\eta' \to \pi^+\pi^-\eta(\eta \to \gamma\gamma)$ decay candidates. The solid curve shows the fit results.

ters of energy deposits in the EMC crystals. The shower energies are required to be greater than 25 MeV for the barrel region ($|\cos\theta| < 0.8$) and 50 MeV for the end-cap region ($0.86 < |\cos\theta| < 0.92$). The showers in the transition region between barrel and end-cap are required to have an energy greater than 100 MeV. Showers must be isolated from all charged tracks by more than 10°.

We require that $\eta(\eta') \to$ invisible events have no charged tracks besides those of the $\phi \to K^+K^-$ candidate. In addition, the number of EMC showers ($N_{\rm shower}$), that could be from a K_L or a photon, are required to

be zero inside a cone of 1.0 rad around the recoil direction against the ϕ candidate. This requirement rejects most η and η' decays into visible final states. It also eliminate most backgrounds from multibody decays of $J/\psi \to \phi$+anything. In order to ensure that η and η' decay particles are inside the fiducial volume of the detector, the recoil direction against the ϕ is required to be within the region $|\cos\theta_{\rm recoil}| < 0.7$, where $\theta_{\rm recoil}$ is the polar angle of the recoil three-momentum of ϕ candidate. Figure 1 (a) shows the K^+K^- invariant mass distribution after the above selection. A clear ϕ peak is seen. Figure 1 (b) shows the recoil mass against ϕ candidates for events with 1.01 GeV/$c^2 < m_{KK} < 1.03$ GeV/c^2, and there are no significant signals in the η and η' mass regions.

We use MC simulated events to determine selection

efficiencies for the signal channels and study possible backgrounds. The efficiencies are 36.0% and 36.1% for η and η' invisible decays, respectively. More than 20 exclusive decay modes are generated with full MC simulations in order to better understand the backgrounds. The sources of backgrounds are divided into two classes. Class I: The background is from $J/\psi \to \phi\eta(\eta')$, where $\phi \to K^+K^-$ and $\eta(\eta')$ decays into visible final states that are not detected by the EMC. The expected number of background events from this class is 0.18 ± 0.02 (1.0 ± 0.2) in the signal region for the $\eta(\eta')$ case. Class II: It is from J/ψ decays to final states without $\eta(\eta')$ or without both $\eta(\eta')$ and ϕ. For the η invisible decay, the dominant background is from $J/\psi \to \gamma\eta_c$, $\eta_c \to K^\pm\pi^\mp K_L$, where the soft radiative photon is either undetected or outside of the 1 rad cone against recoil ϕ direction in the EMC and the fast π is mis-identified as kaon. We determine the expected number of background from $J/\psi \to \gamma\eta_c$, $\eta_c \to K^\pm\pi^\mp K_L$ with a phase space distribution for the $\eta_c \to K^\pm\pi^\mp K_L$ decay in MC simulation, and a systematic uncertainty is assigned to cover the variation due to possible structures on the Dalitz plot. For the η' case, the dominant background is from $J/\psi \to \phi K_L K_L$ and $J/\psi \to \phi f_0(980)$, $f_0(980) \to K_L K_L$. The expected number of background events from class II is 0.8 ± 0.2 and 9.4 ± 1.7 in the signal regions for η and η', respectively.

After all selection criteria are applied, only one event (shown in Fig. 1 (b)) survives in the η signal region where 1.0 ± 0.2 background event is expected. An upper limit (UL) at the 90% confidence level (C.L.) of $N_{\rm UL}^\eta = 3.34$ for $J/\psi \to \phi\eta$ ($\phi \to K^+K^-$ and $\eta \to$ invisible) is obtained using the POLE++ program [30] with the Feldman-Cousins frequentist approach [31]. The information used to obtain the upper limit includes the number of observed events in the signal region, and the expected number of background events and their uncertainty.

For the η' case, an unbinned extended maximum likelihood (ML) fit to the $M_\phi^{\rm recoil}$ distribution in the range 0.8 GeV/$c^2 < M_\phi^{\rm recoil} < 1.2$ GeV/c^2, as shown in Fig. 2, is performed. The signal shape used in the fit, shown in Fig. 3, is obtained from a nearly background-free $J/\psi \to \phi\eta'$, $\eta' \to \pi^+\pi^-\eta$, $\eta \to \gamma\gamma$ sample. The purity of the sample is greater than 98.5%. The shape of the invisible signal peak in the $M_\phi^{\rm recoil}$ distribution is fixed to the smoothed histograms of the $J/\psi \to \phi\eta'$, $\eta' \to \pi^+\pi^-\eta$, $\eta \to \gamma\gamma$ MC sample, and the signal yield is allowed to float. The shape of the dominant background $J/\psi \to \phi f_0(980)$, $f_0(980) \to K_L K_L$ is described by MC simulated data, in which the $f_0(980)$ line shape is parameterized with the Flatté form [32]

$$f(m) = \frac{1}{M_{f_0}^2 + m^2 + i(g_1^2 \rho_{\pi\pi} + g_2^2 \rho_{KK})}, \quad (1)$$

where M_{f_0} is the mass of the $f_0(980)$, m is the effective mass, ρ is Lorentz invariant phase space ($\rho = 2k/m$, here, k refers to the π or K momentum in the rest frame of the resonance), and g_1 and g_2 are coupling-constants for the $f_0(980)$ resonance coupling to the $\pi\pi$ and KK channels, respectively. These parameters [$M_{f_0} = 0.965\pm0.010$ GeV/c^2, $g_1^2 = 0.165 \pm 0.018$ (GeV/c^2)^2 and $g_2^2 = 0.695 \pm 0.075$ (GeV/c^2)^2] have been determined in the analysis of $J/\psi \to \phi\pi^+\pi^-$ and ϕK^+K^- from BESII data [33, 34]. In the ML fit, the dominant background shape ($J/\psi \to \phi f_0(980)$, $f_0(980) \to K_L K_L$) is fixed to the MC simulations, and its yield ($N_{f_0}^{\rm bkg}$) is floated. The shape of the remaining background from $J/\psi \to \phi K_L K_L$ is modeled with a first order Chebychev polynomial whose slope and yield ($N_{\rm non-f_0}^{\rm bkg}$) are floated in the fit to data. The signal yield, $N_{\rm sig}^{\eta'} = 2.3 \pm 4.3$, is consistent with zero observed events, and the resulting fitted values of $N_{f_0}^{\rm bkg}$ and $N_{\rm non-f_0}^{\rm bkg}$ are 239 ± 28 and 37 ± 25, respectively, where the errors are statistical. We obtain an upper limit by integrating the normalized likelihood distribution over the positive values of the number of signal events. The upper limit at the 90% C.L. is $N_{\rm UL}^{\eta'} = 10.1$.

B. Analyses for η and $\eta' \to \gamma\gamma$

The branching fraction of $\eta(\eta') \to \gamma\gamma$ is also determined in $J/\psi \to \phi\eta(\eta')$, in order to obtain the ratio of $\mathcal{B}(\eta(\eta') \to$ invisible$)$ to $\mathcal{B}(\eta(\eta') \to \gamma\gamma)$. The advantage of measuring $\frac{\mathcal{B}(\eta(\eta')\to{\rm invisible})}{\mathcal{B}(\eta(\eta')\to\gamma\gamma)}$ is that the uncertainties due to the total number of J/ψ events, tracking efficiency, PID, the number of the charged tracks, and the residual noise in the EMC cancel.

The selection criteria for the charged tracks are the same as those for $J/\psi \to \phi\eta(\eta')$, $\eta(\eta') \to$ invisible. However, at least two good photons are required. The events are kinematically fitted using energy and momentum conservation constraints (4C) under the $J/\psi \to KK\gamma\gamma$ hypothesis in order to obtain better mass resolution and suppress backgrounds further. We require the kinematic fit $\chi^2_{K^+K^-\gamma\gamma}$ to be less than 90 (40) for the $\eta(\eta')$ case. If there are more than two photons, the fit is repeated using all permutations, and the combination with the best fit to $KK\gamma\gamma$ is retained.

The numbers of $J/\psi \to \phi\eta(\eta')$, $\eta(\eta') \to \gamma\gamma$ events are obtained from an extended unbinned ML fit to the K^+K^- versus $\gamma\gamma$ invariant mass distributions. The projection of the fit on the m_{KK} ($m_{\gamma\gamma}$) axis is shown in Figs. 4(a) and 5(a) (Figs. 4(b) and 5(b)) for the η and η' cases, respectively. In the ML fits, we require that 0.99 GeV/$c^2 < m_{KK} < 1.10$ GeV/c^2 and 0.35 GeV/$c^2 < m_{\gamma\gamma} < 0.75$ GeV/c^2 (0.75 GeV/$c^2 < m_{\gamma\gamma} < 1.15$ GeV/c^2) for the $\eta(\eta')$ case. The signal shape for ϕ is modeled with a relativistic Breit-Wigner (RBW) function [35] convoluted with a Gaussian function that represents the detector resolution; the signal shape for $\eta(\eta')$ is described by a Crystal Ball (CB) function [36], and its parameters are floated. In the ML fits, the width of ϕ is fixed at the PDG value, and its central mass value is floated. The backgrounds are divided into three
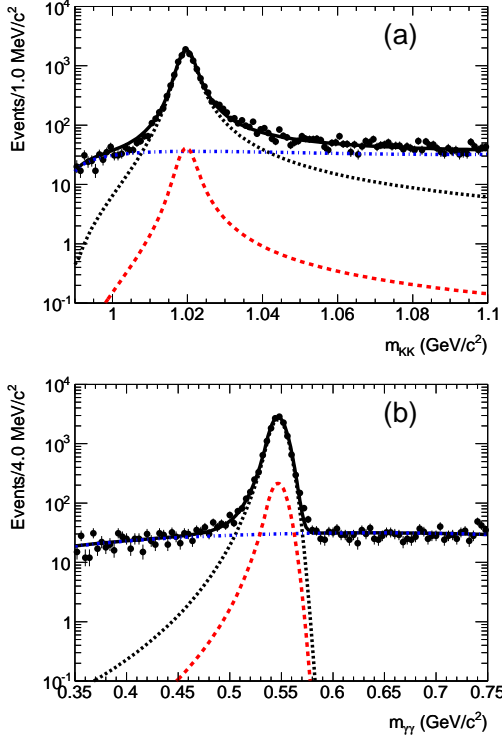
FIG. 4: The (a) m_{KK} and (b) $m_{\gamma\gamma}$ distributions with fit results superimposed for $J/\psi \to \phi\eta$, $\phi \to K^+K^-$, $\eta \to \gamma\gamma$. Points with error bars are data. The (black) solid curves show the results of the fits to signal plus background, and the (black) dashed curves are for signal. In (a), the (blue) dotted-dash curve shows non-ϕ-peaking backgrounds, and the (red) short-dashed curve shows the non-η-peaking background. In (b), the (blue) dotted-dash curve shows non-η-peaking backgrounds, and the (red) short-dashed curve shows the non-ϕ-peaking background.

FIG. 5: The (a) m_{KK} and (b) $m_{\gamma\gamma}$ distributions with fit results superimposed for $J/\psi \to \phi\eta'$, $\phi \to K^+K^-$, $\eta' \to \gamma\gamma$. Points with error bars are data. The (black) solid curves show the results of the fits to signal plus background distributions, and the (black) dashed curves are for signal. In (a), the (blue) dotted-dash curve shows non-ϕ-peaking backgrounds, and the (red) short-dashed curve shows the non-η'-peaking background. In (b), the (blue) dotted-dash curve shows non-η'-peaking backgrounds, and the (red) short-dashed curve shows the non-ϕ-peaking background.

categories: non-$\phi\eta(\eta')$-peaking background (*i.e.*, $J/\psi \to \gamma\pi^0 K^+K^-$, in which one of the photons is missing); non-ϕ-peaking background (*i.e.*, $J/\psi \to K^+K^-\eta(\eta')$); and non-$\eta(\eta')$-peaking background (*i.e.*, $J/\psi \to \phi\gamma\gamma$ and $\phi\pi^0\pi^0$). The probability density functions (PDF) for non-ϕ-peaking background in the m_{KK} distribution is parameterized by [37]

$$B(m_{KK}) = (m_{KK} - 2m_K)^a \cdot e^{-bm_{KK}-cm_{KK}^2}, \quad (2)$$

where a, b and c are free parameters, and m_K is the nominal mass value of the charged kaon from the PDG [28]. The shape for the non-$\eta(\eta')$-peaking background in the $m_{\gamma\gamma}$ distribution is modeled by a second-order Chebychev polynomial function ($B(m_{\gamma\gamma})$). All parameters related to the background shape are floated in the fit to data. The PDFs for signal and backgrounds are combined in the likelihood function $\mathcal{L}$, defined as a function
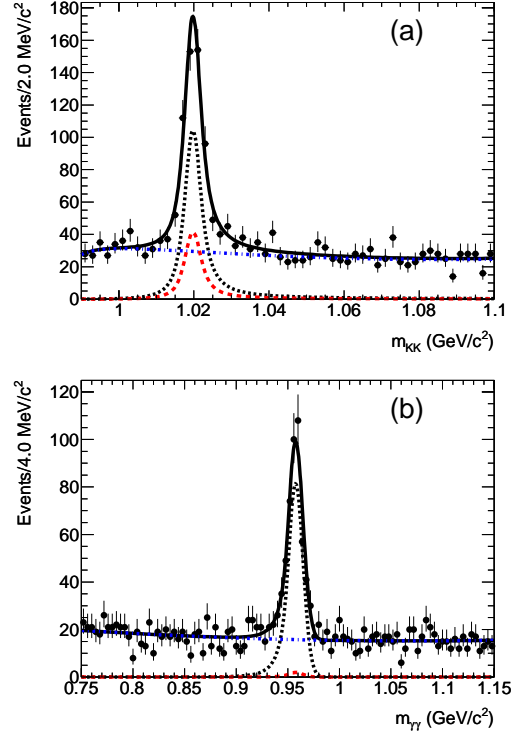
of the free parameters $N_{\gamma\gamma}^{\eta}$, $N_{\mathrm{bkg}}^{\mathrm{non-}\phi\eta}$, $N_{\mathrm{bkg}}^{\mathrm{non-}\phi}$, and $N_{\mathrm{bkg}}^{\mathrm{non-}\eta}$:

$$\mathcal{L} = \frac{e^{-(N_{\gamma\gamma}^{\eta}+N_{\mathrm{bkg}}^{\mathrm{non-}\phi\eta}+N_{\mathrm{bkg}}^{\mathrm{non-}\phi}+N_{\mathrm{bkg}}^{\mathrm{non-}\eta})}}{N!}$$
$$\times \prod_{i=1}^{N}[N_{\gamma\gamma}^{\eta}RBW(m_{KK}^i) \times CB(m_{\gamma\gamma}^i)$$
$$+N_{\mathrm{bkg}}^{\mathrm{non-}\phi\eta}B(m_{KK}^i) \times B(m_{\gamma\gamma}^i)$$
$$+N_{\mathrm{bkg}}^{\mathrm{non-}\phi}B(m_{KK}^i) \times CB(m_{\gamma\gamma}^i)$$
$$+N_{\mathrm{bkg}}^{\mathrm{non-}\eta}RBW(m_{KK}^i) \times B(m_{\gamma\gamma}^i)], \quad (3)$$

where $N_{\gamma\gamma}^{\eta}$ is the number of $J/\psi \to \phi\eta$, $\phi \to K^+K^-$, $\eta \to \gamma\gamma$ events, and $N_{\mathrm{bkg}}^{\mathrm{non-}\phi\eta}$, $N_{\mathrm{bkg}}^{\mathrm{non-}\phi}$, and $N_{\mathrm{bkg}}^{\mathrm{non-}\eta}$ are the numbers of the corresponding three kinds of backgrounds. The fixed parameter N is the total number of selected events in the fit region, and m_{KK}^i ($m_{\gamma\gamma}^i$) is the value of m_{KK} ($m_{\gamma\gamma}$) for the ith event. We use the product of the PDFs, since we have verified that m_{KK} and $m_{\gamma\gamma}$ are uncorrelated for each component. The nega-

tive log-likelihood ($-\ln\mathcal{L}$) is then minimized with respect to the extracted yields. The resulting fitted signal and background yields are summarized in Table I. We also obtain the results for the η' case by replacing η with η' in Eq. (3). The fitted results for $\eta(\eta') \to \gamma\gamma$ are shown in Fig. 4 (Fig. 5). The detection efficiencies are determined with MC simulations to be 36.3% and 31.7% for η and η', respectively.

TABLE I: The fitted signal and background yields for $J/\psi \to \phi\eta(\eta')$, $\eta(\eta') \to \gamma\gamma$, and $\epsilon^{\eta}_{\gamma\gamma}(\epsilon^{\eta'}_{\gamma\gamma})$ is its selection efficiency.

Quantity	Value	
	η	η'
$N^{\eta}_{\gamma\gamma}(N^{\eta'}_{\gamma\gamma})$	13390 ± 136	400 ± 25
$N^{\text{non-}\phi\eta}_{\text{bkg}}(N^{\text{non-}\phi\eta'}_{\text{bkg}})$	2514 ± 64	1482 ± 46
$N^{\text{non-}\phi}_{\text{bkg}}(N^{\text{non-}\phi}_{\text{bkg}})$	1132 ± 70	10 ± 15
$N^{\text{non-}\eta}_{\text{bkg}}(N^{\text{non-}\eta'}_{\text{bkg}})$	313 ± 54	159 ± 26
$\epsilon^{\eta}_{\gamma\gamma}(\epsilon^{\eta'}_{\gamma\gamma})$	36.3%	31.7%

According to the results in Table I, the ratio of $\mathcal{B}(J/\psi \to \phi\eta)$ to $\mathcal{B}(J/\psi \to \phi\eta')$, is found to be consistent with the known value [28]. The individual branching fraction is larger by $1.3(1.6)\sigma$ with respect to the average value listed in Ref. [28] for $\mathcal{B}(J/\psi \to \phi\eta(\eta'))$, while it is consistent with Ref. [17].

IV. SYSTEMATIC UNCERTAINTIES

The contributions to the systematic error on the calculation of the ratios are summarized in Table II. The uncertainty, due to the requirement of no neutral showers in the EMC inside the 1.0 rad cones around the recoil direction against the ϕ candidate, is estimated using the control sample of fully reconstructed $J/\psi \to \phi\eta$, $\eta \to \gamma\gamma$ events. The ratios of events with no extra photons to events without this requirement are obtained for both data and MC simulation. The difference 0.3% is taken as the systematic error for both the η and η' cases. This study determines the difference of the noise in the EMC for MC simulation and data. The uncertainty due to the ϕ mass window requirement is determined to be 1.5% by using the same control sample of $J/\psi \to \phi\eta$, $\eta \to \gamma\gamma$ events.

For the η invisible decay, the dominant background is from $J/\psi \to \gamma\eta_c$, $\eta_c \to K^{\pm}\pi^{\mp}K_L$. The expected number of the background is estimated with the MC simulations using a phase space distribution for $\eta_c \to K^{\pm}\pi^{\mp}K_L$. The uncertainty to the background estimate that covers the variation of the Dalitz plot structures is studied using the data sample of $\psi' \to \gamma\eta_c$, $\eta_c \to K_s K^{\pm}\pi^{\mp}$ events, which were from BESIII in Ref. [38]. The experimental data suggest that the $\eta_c \to K_s K^{\pm}\pi^{\mp}$ decays predominantly via the scalar $K_0^*(1430)$ meson, i.e., $\eta_c \to K_0^*(1430)\bar{K}$,

which is consistent with the results from BABAR and Belle experiments [39, 40]. After correction for detection efficiency, the experimental Dalitz plot distribution in the $\eta_c \to K_s K^{\pm}\pi^{\mp}$ is used to reweight the $\eta_c \to K^{\pm}\pi^{\mp}K_L$ simulation. The reweighting increases the expected number of background events by 5%, which leads to a relative error of 1.2% on $\eta \to$ invisible decay.

For the η' invisible decay, systematic errors in the ML fit originate from the limited number of events in the data sample and from uncertainties in the PDF parameterizations. Since the signal shape is obtained from the $J/\psi \to \phi\eta'$, $\eta' \to \pi^+\pi^-\eta$, $\eta \to \gamma\gamma$ events in the data, the uncertainty due to the signal shape is negligible. The uncertainty due to the background shape is estimated by varying the PDF shape of the background in the ML fit. The shape of the dominant background $J/\psi \to \phi f_0(980)$, $f_0(980) \to K_L K_L$ is parameterized with the Flatté form in Eq. (1). To estimate the uncertainty, we change the central values of the parameters used in the fit by one standard deviation of the measured values [33], and find that the relative error on $\eta' \to$ invisible decay is 1.0%. The systematic uncertainty due to the choice of parameterization for the shape of the background from $J/\psi \to \phi K_L K_L$ is estimated by varying the order of the polynomial in the fit; we find a relative change on the invisible signal yield of 2.9%, which is taken as the uncertainty due to the background model.

The uncertainty in the determination of the number of observed $J/\psi \to \phi\eta(\eta')$, $\phi \to K^+K^-$, $\eta(\eta') \to \gamma\gamma$ events is also estimated. The systematic error due to photon detection is determined to be 1% for each photon [41]. The uncertainty due to the 4C fit is estimated to be 0.4%(0.8%) for the $\eta(\eta')$ case using the control sample $J/\psi \to \pi^0 K^+K^-$. In the fit to the ϕ mass distribution, the mass resolution is fixed to the MC simulation; the level of possible discrepancy is determined with a smearing Gaussian, for which a non-zero σ would represent a MC-data difference in the mass resolution. The uncertainty associated with a difference determined in this way is 0.1% (1.0%) for the $\eta(\eta')$ case. The systematic uncertainty due to the choice of parameterization for the shape of the non-$\phi\eta(\eta')$-peaking background is estimated by varying the order of the polynomial in the fit; we find the relative changes on the $\eta(\eta')$ signal yield of 0.1% (0.6%), which is taken as the uncertainty due to the background shapes. The total systematic errors $\sigma^{\text{sys}}_{\eta}$ and $\sigma^{\text{sys}}_{\eta'}$ on the ratio are 2.8% and 4.1% for η and η', as summarized in Table II.

V. RESULTS

The upper limit at the 90% confidence level on the ratio of $\mathcal{B}(\eta \to \text{invisible})$ to $\mathcal{B}(\eta \to \gamma\gamma)$ is calculated with

$$\frac{\mathcal{B}(\eta \to \text{invisible})}{\mathcal{B}(\eta \to \gamma\gamma)} < \frac{N^{\eta}_{UL}/\epsilon_{\eta}}{N^{\eta}_{\gamma\gamma}/\epsilon^{\eta}_{\gamma\gamma}} \frac{1}{1 - \sigma_{\eta}}, \qquad (4)$$

TABLE II: Summary of errors. The first five lines are relative systematic errors for $J/\psi \to \phi\eta(\eta')$, $\eta(\eta') \to$ invisible. The next four lines are relative systematic errors for $J/\psi \to \phi\eta(\eta')$, $\eta(\eta') \to \gamma\gamma$. The second line from the bottom is the relative statistical error of $N_{\gamma\gamma}^{\eta}(N_{\gamma\gamma}^{\eta'})$.

	Sys. error (%)	
Source of uncertainties	η	η'
Requirement on N_{shower}	0.3	0.3
ϕ mass window	1.5	1.5
$J/\psi \to \gamma\gamma\eta_c$, $\eta_c \to K_L K^\pm \pi^\mp$ background	1.2	-
Background shape of $J/\psi \to \phi f_0(980)$	-	1.0
Background shape of $J/\psi \to \phi K_L K_L$	-	2.9
4C fit for $\eta(\eta') \to \gamma\gamma$	0.4	0.8
Photon detection	2.0	2.0
Signal shapes for $\eta(\eta') \to \gamma\gamma$	0.1	1.0
Background shape for $\eta(\eta') \to \gamma\gamma$	0.1	0.6
Total systematic errors	2.8	4.1
Statistical error of $N_{\gamma\gamma}^{\eta}(N_{\gamma\gamma}^{\eta'})$	1.0	6.0
Total errors	3.0	7.4

where N_{UL}^{η} is the 90% upper limit of the number of observed events for $J/\psi \to \phi\eta$, $\phi \to K^+K^-$, $\eta \to$ invisible decay, ϵ_η is the MC determined efficiency for the signal channel, $N_{\gamma\gamma}^{\eta}$ is the number of events for the $J/\psi \to \phi\eta$, $\phi \to K^+K^-$, $\eta \to \gamma\gamma$, $\epsilon_{\gamma\gamma}^{\eta}$ is the MC determined efficiency, and σ_η is the total error for the η case from Table II. The upper limit on the ratio of $\mathcal{B}(\eta' \to \text{invisible})$ to $\mathcal{B}(\eta' \to \gamma\gamma)$ is obtained similarly. Since only the statistical error is considered when we obtain the 90% upper limit of the number of events, to be conservative, N_{UL}^{η} and $N_{UL}^{\eta'}$ are shifted up by one sigma of the additional uncertainties (σ_η or $\sigma_{\eta'}$).

Thus, the upper limit of 2.6×10^{-4} (2.4×10^{-2}) on the ratio of $\mathcal{B}(\eta(\eta') \to \text{invisible})$ and $\mathcal{B}(\eta(\eta') \to \gamma\gamma)$ is obtained at the 90% confidence level.

VI. CONCLUSION

In summary, the invisible decays of η and η' are searched for in the two-body decays $J/\psi \to \phi\eta$ and $\phi\eta'$ using $(225.3 \pm 2.8) \times 10^6$ J/ψ decays collected with the BESIII detector. We find no signal above background for the invisible decays of η and η' and obtain upper limits at the 90% C.L. of 2.6×10^{-4} and 2.4×10^{-2} for

$\frac{\mathcal{B}(\eta \to \text{invisible})}{\mathcal{B}(\eta \to \gamma\gamma)}$ and $\frac{\mathcal{B}(\eta' \to \text{invisible})}{\mathcal{B}(\eta' \to \gamma\gamma)}$, respectively. Using the branching fraction values of η and $\eta' \to \gamma\gamma$ from the PDG [28], we determine the invisible decay rates to be $\mathcal{B}(\eta \to \text{invisible}) < 1.0 \times 10^{-4}$ and $\mathcal{B}(\eta' \to \text{invisible}) < 5.3 \times 10^{-4}$ at the 90% confidence level.

Our limits are improved by factors of 6 and 3 compared to the previous ones obtained at BESII [17], the η' limit being almost 2 times better than the recent one from the CLEO-c experiment [18]. The limit for $\eta \to$ invisible is smaller than a tentative estimate [13] for the $\eta \to \chi\chi$ decay to a pair of light dark matter particles, no such decays, however, being expected from the virtual exchanges of a spin-1 U boson (or dark photon) with vector couplings to quarks. These limits constrain the decays $\eta(\eta') \to UU$ where each U decays invisibly into neutrinos or LDM, with branching fraction B_{inv}. The resulting $\eta(\eta')$ limits on the U couplings to quarks are improved by $\simeq 1.6$ and 1.3 as compared to those obtained in [2] from the BESII limits [17], and now read $\sqrt{f_u^2 + f_d^2} < 3 \times 10^{-2}/\sqrt{B_{\text{inv}}}$ and $|f_s| < 4 \times 10^{-2}/\sqrt{B_{\text{inv}}}$, respectively (for $2m_U$ smaller than m_η or $m_{\eta'}$ and not too close to them), f_u, f_d and f_s denoting effective couplings of the U boson to light quarks.

[1] P. Fayet, Phys. Lett. B **84**, 421 (1979); P. Fayet and J. Kaplan, Phys. Lett. B **269**, 213 (1991); B. McElrath, Phys. Rev. D **72**, 103508 (2005).

[2] P. Fayet, Phys. Rev. D **74**, 054034 (2006).

[3] P. Fayet, Phys. Rev. D **81**, 054025 (2010).

[4] F. Wilczek, Phys. Rev. Lett. **40**, 279 (1978); S. Weinberg, Phys. Rev. Lett. **40**, 223 (1978).

[5] P. Fayet, Nucl. Phys. B **187**, 184 (1981); Phys. Lett. B **675**, 267 (2009).

[6] P. Fayet, Phys. Rev. D **75**, 115017 (2007).

[7] C. Edwards *et al.*, Phys. Rev. Lett. **48**, 903 (1982).

[8] R. Balest *et al.* (CLEO Collaboration), Phys. Rev. D **51**, 2053 (1995).

[9] J. Insler *et al.* (CLEO Collaboration), Phys. Rev. D **81**, 091101(R) (2010).

[10] C. Boehm and P. Fayet, Nucl. Phys. B **683**, 219 (2004); P. Fayet, Phys. Rev. D **70**, 023514 (2004).

[11] C. Boehm, D. Hooper, J. Silk, M. Casse, and J. Paul, Phys. Rev. Lett. **92**, 101301 (2004); J. F. Beacom, N. F. Bell, and G. Bertone, Phys. Rev. Lett. **94**, 171301 (2005); N. Borodatchenkova, D. Choudhury, and M. Drees, Phys. Rev. Lett. **96**, 141802 (2006).

[12] P. Jean *et al.*, Astron. Astrophys. **407**, L55 (2003); SPI is the spectrometer aboard INTEGRAL.

[13] B. McElrath, arXiv:0712.0016[hep-ph], *Proceedings of the CHARM 2007 Workshop*, Ithaca, NY, August 5-8, 2007.

[14] P. Fayet, Nucl. Phys. B **347**, 743 (1990).

[15] H. B. Li and T. Luo, Phys. Lett. B **686**, 249 (2010).

[16] A. V. Artamonov *et al.* (E949 Collaboration), Phys. Rev. D **72**, 091102 (2005).

[17] M. Ablikim *et al.* (BES Collaboration), Phys. Rev. Lett. **97**, 202002 (2006).

[18] P. Naik *et al.* (CLEO Collaboration), Phys. Rev. Lett. **102**, 061801 (2009).

[19] M. Ablikim *et al.* (BES Collaboration), Phys. Rev. Lett. **100**, 192001 (2008).

[20] B. Aubert *et al.* (BABAR Collaboration), Phys. Rev. Lett. **103**, 251801 (2009); P. Rubin *et al.* (CLEO Collaboration), Phys. Rev. D **75**, 031104 (2007); O. Tajima *et al.* (Belle Collaboration), Phys. Rev. Lett. **98**, 132001 (2007).

[21] A. R. Fazely *et al.*, Phys. Rev. D **81**, 117101 (2010).

[22] M. Ablikim *et al.* (BESIII Collaboration), Chinese Physics C **36**, 915 (2012).

[23] M. Ablikim *et al.* (BESIII Collaboration), Nucl. Instrum. Meth. A **614**, 345 (2010).

[24] D. M. Asner *et al.*, Int. J. Mod. Phys. A **24**, Supp. (2009).

[25] S. Agostinelli *et al.* (GEANT4 Collaboration), Nucl. Instrum. Meth. A **506**, 250 (2003).

[26] S. Jadach, B. F. L. Ward and Z. Was, Comput. Phys. Commun. **130**, 260 (2000); S. Jadach, B. F. L. Ward and Z. Was Phys. Rev. D **63**, 113009 (2001).

[27] D. J. Lange, Nucl. Instrum. Meth. A **462**, 152 (2001).

[28] J. Beringer *et al.* (Particle Data Group), Phys. Rev. D **86**, 010001 (2012).

[29] J. C. Chen, G. S. Huang, X. R. Qi, D. H. Zhang, and Y. S. Zhu, Phys. Rev. D **62**, 034003 (2000).

[30] J. Conrad, O. Botner, A. Hallgren and C. Peréz de los Heros, Phys. Rev. D **67**, 012002 (2003); http://polepp.googlecode.com/svn/tags/POLEPP-1.1.0.

[31] G. J. Feldman and R. D. Cousins, Phys. Rev. D **57**, 3873 (1998).

[32] S. M. Flatté, Phys. Lett. B **63**, 224 (1976).

[33] M. Ablikim *et al.* (BES Collaboration), Phys. Lett. B **607**, 243 (2005).

[34] It is noted that diffrent definition of Flatté form is used in Eq. (1) in Ref. [33]. Here, g_1^2 and g_2^2 are identical to 'g_1' and 'g_2' in Ref. [33]. Therefore, we notice that the unit for the 'g_1' and 'g_2' in Ref. [33] should be $(\text{GeV}/c^2)^2$ instead of GeV/c^2.

[35] F. von Hippel and C. Quigg, Phys. Rev. D **5**, 624, (1972); J. Blatt and V. Weisskopf, *Theoretical Nuclear Physics*, New York: John Wiley & Sons (1952).

[36] J. E. Gaiser, Ph. D. Thesis, SLAC-R-255 (1982) (unpublished); M. J. Oreglia, Ph. D. Thesis, SLAC-R-236 (1980) (unpublished); T. Skwarnicki, Ph. D. Thesis, DESY-F-31-86-02 (1986) (unpublished).

[37] C. C. Chang *et al.* (E580 Collaboration), Phys. Rev. D **29**, 1888 (1984); D. Barberis *et al.* (WA102 Collaboration), Phys. Lett. B **436**, 204 (1998).

[38] M. Ablikim *et al.* (BESIII Collaboration), Phys. Rev. Lett. **108**, 222002 (2012).

[39] J. P. Lees *et al.* (BABAR Collaboration), Phys. Rev. D **81**, 052010 (2010).

[40] A. Vinokurova *et al.* (Belle Collaboration), Phys. Lett. B **706**, 139 (2011).

[41] M. Ablikim *et al.* (BESIII Collaboration), Phys. Rev. D **83**, 112005 (2011).